Sulphur isotope stratigraphy of drill cuttings and stratigraphic correlation of Permian-Triassic evaporites

Jack Salisbury[1]*, Darren R. Gröcke[1]* and Tom McKie[2]

[1]Stable Isotope Biogeochemistry Laboratory (SIBL), Department of Earth Sciences, Durham University, Durham, United Kingdom, [2]Shell UK Exploration and Production, Aberdeen, United Kingdom

The stratigraphy of the European late Permian-Triassic commonly lacks chronostratigraphic constraint due to the scarcity of diagnostic fossils for biostratigraphy. This is particularly true for the United Kingdom, and as a result, stratigraphic correlation within and between sedimentary basins is primarily reliant on lithostratigraphy. Evaporitic sulphate can be used to develop time series of $\delta^{34}S_{evap}$ data that can be utilised for stratigraphic correlation. However, the availability of continuous drillcore is limited, whilst drill cuttings are commonly acquired but are widely overlooked for stable isotope stratigraphy. We derive a $\delta^{34}S_{evap}$ record from drill cuttings from the southern North Sea Basin, and successfully correlate it with an equivalent published $\delta^{34}S_{evap}$ record from a continuous drillcore in the Cleveland Basin, Yorkshire, United Kingdom. We have chosen seven points in the $\delta^{34}S_{evap}$ records for stratigraphic correlation, defining eight packages of isotopically distinct coeval strata. This is significant, as the ubiquity of drill cuttings presents the opportunity to derive $\delta^{34}S_{evap}$ curves with high geospatial resolution. Equivalent gamma ray logs were used for correlation and compared with the $\delta^{34}S_{evap}$ curves. The correlations agree relatively well, however, the $\delta^{34}S_{evap}$ correlation permits the development of more robust chronostratigraphic constraints. Specifically, the $\delta^{34}S_{evap}$ records constrain the age of the Bunter Shale and Bunter Sandstone in the western Southern North Sea to the latest Permian. This has significant implications for understanding the stratigraphy and palaeogeographic evolution of United Kingdom Permian-Triassic sedimentary basins, and may have economic implications, since the Bunter Sandstone is being considered as a potential reservoir for CO_2 storage in the United Kingdom sector.

KEYWORDS

sulphur isotopes, stratigraphy, lithostratigraphy, Mercia Mudstone Group, evaporites, drill cuttings, gamma ray, Permian-Triassic

1 Introduction

The late Permian and Triassic time intervals have received a great deal of interest over the past 50 years, due to numerous events of geological significance, most notably the End Permian Mass Extinction (EPME) and the End Triassic Extinction (ETE) — two of the 'Big Five' extinction events (Raup and Sepkoski, 1982; Sepkoski, 1996). Both the Permian–Triassic boundary (PTB) interval and the ETE are associated with major biogeochemical perturbations. In particular, the sulphur cycle exhibits significant shifts in the sulphur isotopic composition ($\delta^{34}S$) of seawater sulphate (Newton et al., 2004; Horacek

et al., 2010; Bernasconi et al., 2017; He et al., 2020). Despite this knowledge, high-resolution $\delta^{34}S$ records remain sparse between these major extinction events, with many studies focusing primarily on specific, short intervals of time, such as the PTB (Newton et al., 2004; Schobben et al., 2015) and the Early Triassic (Lyu et al., 2019; Song et al., 2019). The sedimentary environment for much of the European Permo-Triassic was arid and continental (with episodic marine influence) (Kutzbach and Gallimore, 1989; Parrish, 1993), characterised by abundant evaporite-bearing sediments (McKie, 2017). Thus, these evaporitic sedimentary sequences may provide an ideal opportunity to generate marine $\delta^{34}S_{evap}$ records for correlation.

Stable isotope stratigraphy has been successful in deriving chronostratigraphic correlations at high resolution (e.g., Jenkyns et al., 2002; Korte and Kozur, 2010; Yao, et al., 2019; Paytan et al., 2020). Specifically, carbon isotope stratigraphy has been applied using marine and terrestrial organic matter and carbonate (see Gröcke, 2020). In addition, sulphur isotope stratigraphy has also proved successful for correlation using marine evaporites, barite and carbonate-associated sulphate (CAS) ($\delta^{34}S_{evap}$, $\delta^{34}S_{barite}$, $\delta^{34}S_{CAS}$, respectively: see review by Paytan et al., 2020). Despite the high-resolution achieved with $\delta^{34}S_{barite}$ records (Paytan et al., 1998; 2004; 2012; Markovic et al., 2015; Yao et al., 2018; 2020), barite is predominantly acquired from pelagic sediments, and thus only provides insight into the previous 130 million years (Yao et al., 2019). Although $\delta^{34}S_{CAS}$ records have been widely employed to understand the ancient sulphur cycle (e.g., Newton et al., 2004; Luo et al., 2010; Song et al., 2014; Crockford et al., 2019; He et al., 2019; 2020), their suitability as a stratigraphic and palaeoenvironmental tool is under scrutiny due to issues of diagenesis (Rennie and Turchyn, 2014; Present et al., 2015; 2019; Richardson et al., 2019; 2021; Murray et al., 2021; Bryant et al., 2022). Accordingly, much of the variability in $\delta^{34}S_{CAS}$ across the PTB and Early Triassic has been attributed to post-depositional alteration (Bernasconi et al., 2017; Johnson et al., 2021). Therefore, it would conclude that evaporites are the most reliable proxy to generate pre-Cretaceous global marine $\delta^{34}S$ curves.

The $\delta^{34}S$ of marine sedimentary sulphates (e.g., evaporites) is assumed to be indicative of coeval seawater sulphate. The respective contributions and isotopic composition of sulphur fluxes entering and leaving the ocean reservoir act to control the $\delta^{34}S$ of seawater sulphate ($\delta^{34}S_{sulphate}$) over geologic time (Paytan et al., 2012; 2020; Bernasconi et al., 2017; Crockford et al., 2019). It is generally assumed that for much of the Phanerozoic, oceanic sulphate has largely remained well-mixed and isotopically homogenous (Paytan et al., 2012; Present et al., 2020). Therefore, coeval sedimentary sulphates will exhibit comparable absolute $\delta^{34}S_{sulphate}$ values, providing high-resolution stratigraphic correlation across sedimentary basins, especially over periods of significant isotopic change (Yao et al., 2019; Paytan et al., 2020): for example, over the PTB interval (e.g., Claypool et al., 1980; Bernasconi et al., 2017).

The late Permian–Early Triassic time interval is associated with a major perturbation in the sulphur cycle, that is characterised by a rapid increase in the $\delta^{34}S$ of seawater sulphate (recorded in $\delta^{34}S_{CAS}$ and $\delta^{34}S_{evap}$) from ~+12‰ in the late Permian to >+30‰ in the earliest Triassic (Newton et al., 2004; Insalaco et al., 2006; Horacek et al., 2010; Luo et al., 2010; Song et al., 2014; Schobben et al., 2015; Bernasconi et al., 2017). This major positive $\delta^{34}S$ excursion has been

interpreted as a result of an enhanced pyrite burial flux, related to the expansion of ocean anoxia after the emplacement of the Siberian Traps large igneous province in the late Permian (Newton et al., 2004; Bernasconi et al., 2017; Salisbury et al., 2022). Bernasconi et al. (2017) compiled and produced a $\delta^{34}S_{evap}$ record from the latest Permian to the Middle/Late Triassic from multiple sedimentary basins. The resultant $\delta^{34}S_{evap}$ curve showed that the record was not erratic in nature, but changed systematically through time, and hence could be used for stratigraphic correlation: as previously indicated for $\delta^{34}S_{barite}$ (Paytan et al., 1998; 2004; 2012; 2020). Salisbury et al. (2022) produced a high-resolution $\delta^{34}S_{evap}$ curve for the Middle and Late Triassic using evaporitic minerals (e.g., gypsum, anhydrite, halite) from a continuous drillcore, Staithes S-20 borehole, in Yorkshire, England. This updated $\delta^{34}S_{evap}$ record revealed a new, prominent negative excursion of ~10‰ at the Olenekian/Anisian boundary (Salisbury et al., 2022). Although the mechanism for this excursion is currently unclear, one possibility is a weathering pulse, interrupting the pyrite burial event with an influx of isotopically light sulphur (Salisbury et al., 2022). The $\delta^{34}S_{evap}$ curve quickly recovers in the earliest Anisian to pre-excursion values after which it exhibits a gradual decline for the remainder of the Triassic to the Norian/Rhaetian boundary (Salisbury et al., 2022). The global $\delta^{34}S_{evap}$ curve produced in Salisbury et al. (2022) will provide a basis from which to correlate other sedimentary sequences and basins for the Triassic.

In the Triassic strata of the United Kingdom, laterally extensive evaporite beds are used to correlate within and between sedimentary basins based primarily upon the principles of lithostratigraphy (Warrington et al., 1980). The validity of this approach, in some cases, is questionable, especially when correlating between a chain of halite-bearing basins, as a hydrologically restricted basin cannot, by definition, export brines to an adjacent basin in the chain (Warren, 2006). This, and the diachroneity of lithostratigraphic boundaries, limits the validity of lithostratigraphic correlations in deriving a robust chronostratigraphic framework for the Permian–Triassic in the United Kingdom.

Boreholes offer a continuous, unweathered stratigraphic interval and are thus preferable to outcrop (e.g., Staithes S-20). However, only partial cores are usually taken, primarily due to limited time and costs, and the perceived lack of value of information collected outside the economic target interval. In contrast, drill cuttings, depending on the drilling technique used, are commonly collected and retained. If one could analyse drill cuttings and create a similar long-term $\delta^{34}S_{evap}$ curve, then it would offer the potential to produce more stratigraphic records geo-spatially and thus, generate a more robust temporal record for stratigraphic correlation. Ultimately, this approach could be developed in conjunction with biostratigraphy, chemostratigraphy (Metzger et al., 2014; Eldrett et al., 2021) and magnetostratigraphy when possible.

Although promising, drill cuttings present other issues that require consideration, including sampling density, caving, and contamination. Cuttings are collected in batches that reflect an average depth interval, which will vary in resolution depending on drilling and sampling rates. In addition, the integrity of samples from a specific depth may prove questionable, due to the mixing of fragments during the extraction process. Mixing can occur via caving, whereby cuttings from higher stratigraphic levels combine
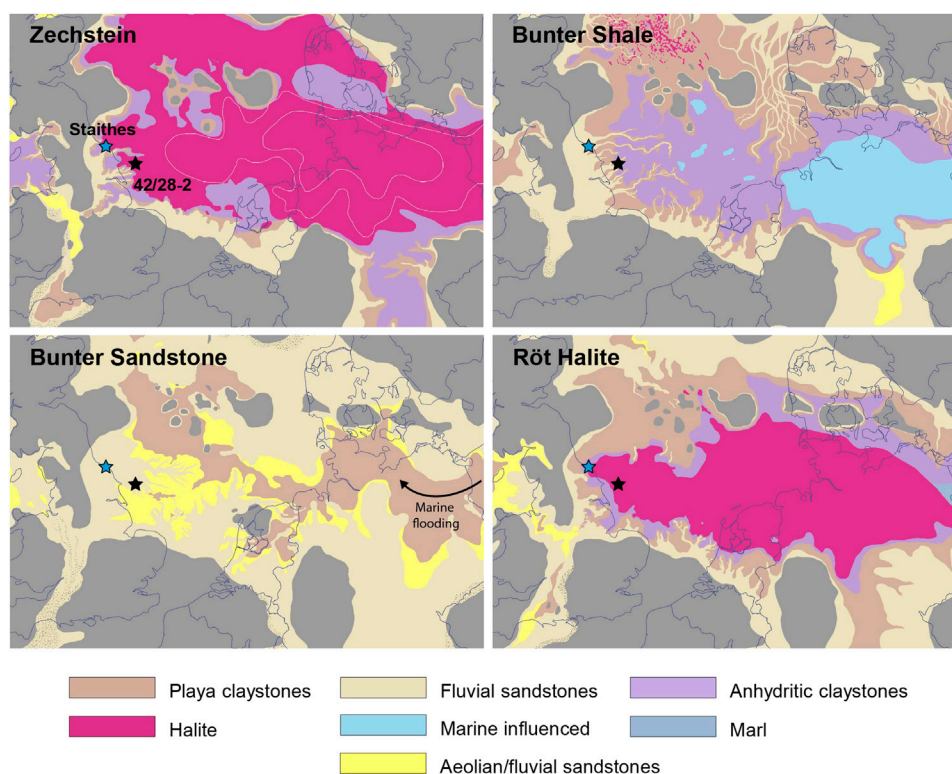
FIGURE 1
Palaeogeographic context of the stratigraphic units discussed in the text. The location of each borehole is marked with a star. See top left figure for labels.

with those at a deeper level where the drill bit is located, or through mixing within the drilling fluid as it is returned to the surface. Drilling fluids may also contaminate samples for specific types of chemical analyses (Kubo et al., 2016). However, recent studies have demonstrated the validity of drill cuttings for carbon isotope stratigraphy, in part through comparison with $\delta^{13}C$ records from cored intervals and outcrop (Metzger et al., 2014; Eldrett et al., 2021). Sanei et al. (2020) demonstrated that with sufficient cleaning of drill cuttings, total organic carbon (TOC) values are comparable to those directly obtained from cored intervals. To our knowledge, only a single study has demonstrated the suitability of borehole cuttings for sulphur isotope stratigraphy (Cao et al., 2016), however, the authors did not demonstrate the validity of drill cuttings for evaporitic lithologies.

In this study, we targeted drill cuttings from an offshore southern North Sea Basin borehole (42/28-2) that spans the late Permian to Late Triassic time interval (Figure 1). This borehole was chosen primarily because lithostratigraphic correlation suggests it spans a stratigraphic interval equivalent to that of the Staithes S-20 borehole (Salisbury et al., 2022). The primary aim of this study was to determine if drill cuttings through an evaporite-bearing sedimentary sequence can be used for sulphur isotope stratigraphy. We successfully correlate the $\delta^{34}S_{evap}$ curve generated from drill cuttings at site 42/28-2 to the Staithes S-20 curve, demonstrating the validity of drill cuttings for correlation between sedimentary basins. Thus, although we advise that future studies should always consider the impact of drilling fluids and post-

drilling washing techniques, the excellent correlation between 42/28-2 and Staithes S-20 suggests they had little effect on $\delta^{34}S_{evap}$ values (in this study).

2 Geological setting

During the late Permian and Triassic, Britain was located at a palaeolatitude of ~20 °N (Newell, 2018), and deposition occurred under a largely arid to semi-arid climate (McKie and Williams, 2009) conducive to evaporite deposition (Figure 1). Late Permian rifting provided the Boreal ocean with restricted access to the subsiding southern Permian Basin (Smith, 1989; McKie, 2017), facilitating the deposition of the Zechstein carbonate-evaporite cycles. Ongoing rifting during the Triassic subsequently opened access routes to the south, allowing ingress of Tethyan seawater into the southern Permian Basin (McKie, 2017). In this study, we focused on the time interval that spans from the uppermost Zechstein (Changhsingian–latest Permian) through to the offshore equivalent of the Keuper Marl of the Mercia Mudstone Group (MMG), the Triton and Dudgeon formations (Norian, Late Triassic) (Figure 2).

In total, the Zechstein is composed of seven carbonate-evaporite cycles (Tucker, 1991). In this study, the uppermost Zechstein is represented in both boreholes as thick-bedded halite. Overlying the Zechstein evaporites are the terminal splay/playa deposits of the Bunter Shale, followed by the Bunter Sandstone—the offshore equivalent of the Sherwood
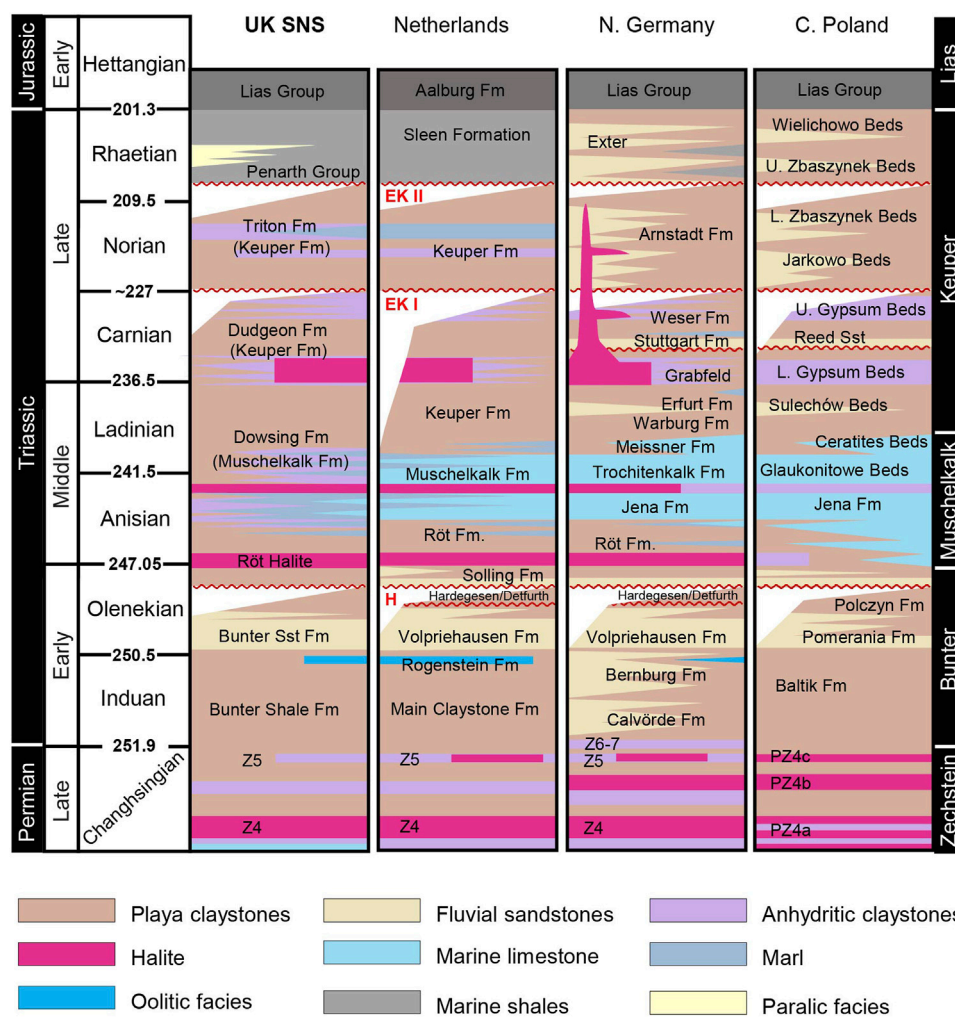
FIGURE 2
The established lithostratigraphic framework for the UK Southern North Sea (SNS), and neighbouring regions with equivalent strata, including the Netherlands, northern Germany, and Poland. The major lithostratigraphic units are provided, along with the regional names and stratigraphic position of rock formations. H marks the base of the Solling (Hardegesen) Unconformity. EK I and II denote the early Kimmerian unconformities. Chronology follows Salisbury et al. (2022).

Sandstone Group (SSG) of eastern England (Noy et al., 2012). The latter is predominantly composed of arenaceous sandstones, largely representing a fluvial-aeolian depositional regime (Ambrose et al., 2014; McKie, 2017). Monsoonal rainfall on the Variscan mountains and smaller basement massifs fed extensive braided river systems (Geluk et al., 2018) that flowed towards basin centre playa and sabkha (Figure 1). However, intermittent periods of aridity suppressed fluvial deposition rates and facilitated aeolian reworking (McKie, 2017). Biostratigraphic age constraints suggest a Middle Triassic (Anisian) age for the Otter Sandstone (Sherwood Sandstone Group) in Devon (Holloway et al., 1989; Spencer and Storrs, 2002) and an Early Triassic age for the Buntsandstein and its' equivalents in continental Europe (Scholze et al., 2016; 2017). However, such constraints are lacking for the Bunter Sandstone in the Cleveland and SNS basins (Warrington et al., 1980).

The SSG is overlain by the MMG (and offshore equivalents), with the boundary being marked by the transition from sandstones to mudstones (Howard et al., 2008; Newell et al., 2018). The MMG is composed of green/grey mudstones interbedded with siltstone, and bedded halite is interspersed with nodular gypsum and anhydrite throughout the succession. In the United Kingdom sector, deposition coincided with the southerly retreat of the SSG beginning in the Middle Triassic, with fluvial systems replaced by a hypersaline playa lake and coastal sabkha environment (Howard, 2008) (Figure 1). This environmental shift facilitated the deposition of evaporites, including bedded halites (i.e., the Röt) and nodular sulphates. Episodic marine flooding during the Anisian and Ladinian is evidenced by acritarchs and lingula in various locations (Warrington, 1974; Wilson, 1993; Ambrose and Wakefield, 2015; Warrington and Pollard, 2021). Evaporite formation and deposition continued intermittently until the latest Triassic. During the latest Triassic, a major marine transgression occurred (Peacock, 2004) leading to the deposition of the Penarth Group (Lott and Warrington, 1988;

Warrington and Ivimey-Cook, 1992; Gallois, 2009), that is biostratigraphically constrained to the Rhaetian (Lott and Warrington, 1988; Warrington, 1997; Hounslow and Ruffell, 2006). This interval represents the transition from marginal marine to fully marine deposition, which became well established during the Hettangian with the deposition of the Lias Group (Wignall and Bond, 2008; Gallois, 2009).

Despite intensive study, the units of the SSG and MMG commonly lack any age-diagnostic fossils for biostratigraphic constraint and hence, dominantly rely on lithostratigraphy. Although, the marine Triassic stratigraphy of continental Europe (i.e., Muschelkalk) is aided by biostratigraphic constraints (Narkiewicz, 1999; Márquez-Aliaga et al., 2000; Bachman and Kozur, 2004; Franz et al., 2013; Chen et al., 2019), the United Kingdom sector facies are particularly impoverished in age-diagnostic fossils, in part due to the lack of marine carbonates when compared with continental Europe (e.g., Horacek et al., 2010; Boschetti et al., 2011). As a result, it is common for this region to lack sufficient chronostratigraphic calibration for the Triassic interval (McKie and Williams, 2009). Therefore, alternative techniques are required to constrain and corroborate the Triassic lithostratigraphic framework of northwest Europe (especially the United Kingdom) with continental Europe. Due to the presence of evaporite minerals throughout the MMG, sulphur isotope stratigraphic correlation is an ideal candidate to address this issue.

3 Methods

Gamma ray data were obtained for boreholes Staithes S-20 (NZ71NE/14; grid reference, NZ 476034E 518000N) and 42/28-2 (54.078556, 0.454889). The onshore Staithes S-20 borehole is located in the Cleveland Basin, England, whereas borehole 42/28-2 is located offshore in the southern North Sea (Figure 1). The sulphur isotope record of Staithes S-20 is presented in Salisbury et al. (2022). Borehole drill cuttings from 42/28-2 were sampled at the British Geological Survey, Keyworth, Nottingham. The washed drill cuttings were collected at variable depth intervals, providing a total of 50 samples for sulphur isotope analysis. The sampling resolution varies throughout the borehole, depending on the abundance of evaporite minerals suitable for sampling. Each sample represents a depth range and is thus viewed as a lithological average over that depth interval.

Each drill cutting sample was inspected under an optical microscope and individual random chips of gypsum, anhydrite and/or halite were picked and transferred into 1.5 mL micro-centrifuge tubes. Approximately 1–3 g of evaporite samples were placed into a 15 mL centrifuge tube with 10% NaCl solution. Blanks of NaCl produced no visible barium sulphate ($BaSO_4$). The evaporites were left to sit in the solution for between 24–48 h and agitated every few hours during the working day. Upon dissolution, the samples underwent centrifugation for 5 min at 3,000 rpm, before the supernatant was poured into 50 mL centrifuge tubes for subsequent $BaSO_4$ precipitation. Between 15–20 mL of 10% barium chloride ($BaCl_2$) was added to the evaporite-dissolved solution. This solution often turned cloudy immediately indicating that $BaSO_4$ was being precipitated, according to the following equation:

$$BaCl_2 + SO_4^{2-} \rightarrow BaSO_4 + 2Cl^{2-} \qquad (1)$$
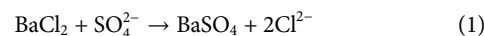
The pH of the solution was reduced to ~1–2 with the addition of 3M HCl to prevent the precipitation of barium carbonate ($BaCO_3$). The samples were left for at least 24 h for $BaSO_4$ precipitation, after which they were centrifuged at 3,000 rpm for 5 min. The $BaCl_2$/HCl supernatant was discarded according to safety regulations for appropriate waste disposal. The resultant pellet of $BaSO_4$ was rinsed with ~30–40 mL of deionised water to neutralise the sample. Neutrality was often achieved after three rinses. The centrifuge tube containing the $BaSO_4$ was placed in a drying oven set at 80°C for between 24 and 48 h. The $BaSO_4$ was then crushed into a fine powder using an agate pestle and mortar and archived in a 1.5 mL micro-centrifuge tube.

For sulphur isotope analysis, each sample was weighed out (0.2–0.4 mg) into 6×4 tin capsules. Stable sulphur isotope analysis was performed in the Stable Isotope Biogeochemistry Laboratory (SIBL) at Durham University using a Thermo Scientific EA IsoLink™ coupled to a Thermo Scientific Delta V Plus isotope-ratio mass-spectrometer. Evaporite sulphur isotope ratios are expressed in standard delta (δ) notation in per mil (‰) relative to Vienna Canyon Diablo Triolite (VCDT) according to the following equation:
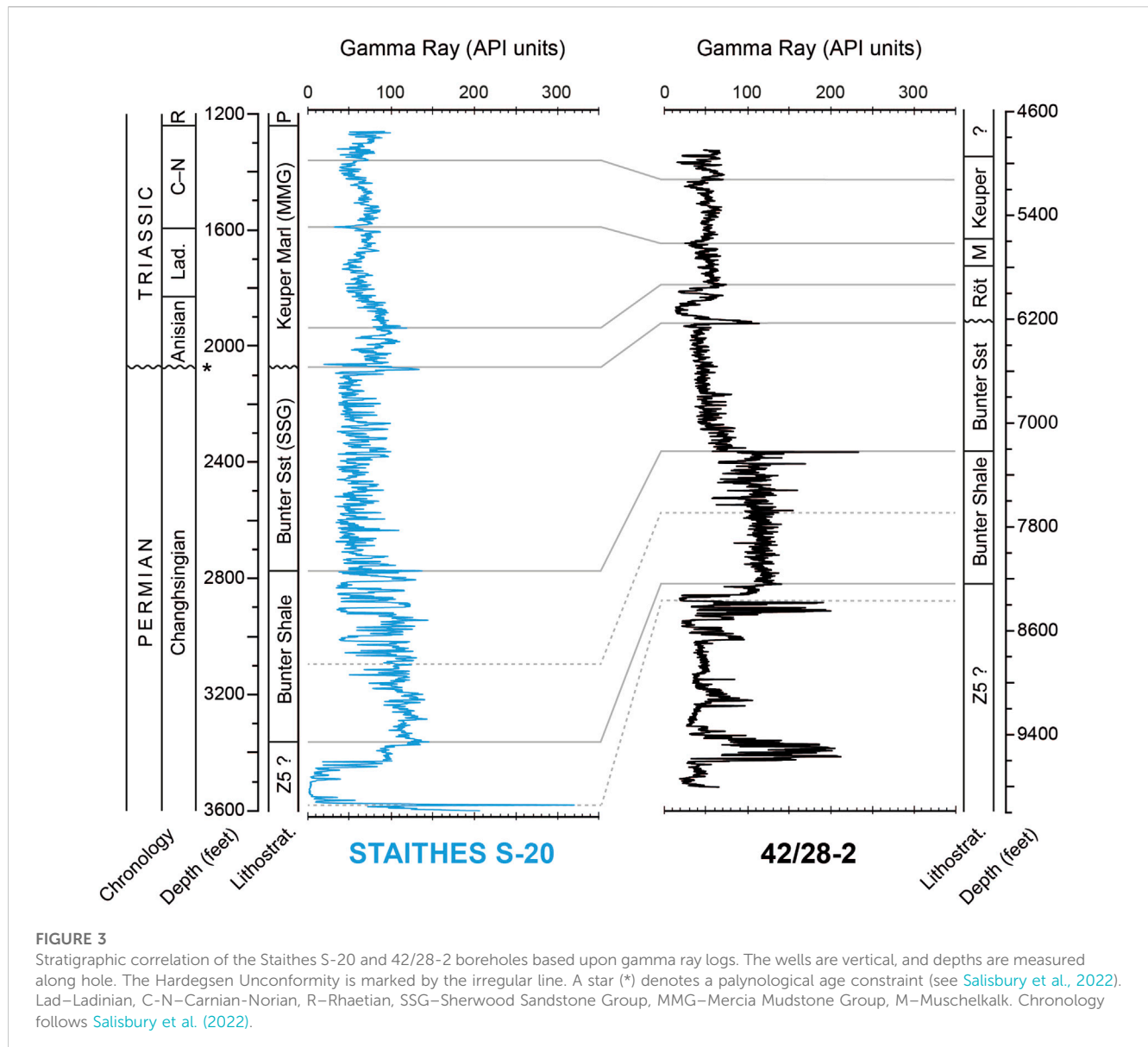
$$\delta^{34}S = \left[\frac{\left((^{34}S/^{32}S)_{sample} - (^{34}S/^{32}S)_{VCDT} \right)}{(^{34}S/^{32}S)_{VCDT}} \right] * 1000 \qquad (2)$$

The $\delta^{34}S$ data were normalised through calibration against four international standards (IAEA-S-1, IAEA-S-2, IAEA-S-3, NBS 127), providing a linear range in $\delta^{34}S$ between −32.5‰ and +22.6‰. An internal barium sulphate (Acros Organics silver sulphate, Catalogue number: 194070100, lot: A0384698) was analysed throughout the analytical period and produced an average $\delta^{34}S$ value of −18.1‰ ± 0.25 (1σ) (n = 14). Analytical uncertainty of $\delta^{34}S$ was ±0.15‰ (1 σ) for replicate analyses of the international standards during the production of this dataset. Reproducibility of sample $\delta^{34}S_{evap}$ was the same or better. Total sulphur of the sample is calculated as part of the isotopic analysis using an internal standard, sulphanilamide (S = 18.619%).

4 Results/discussion

4.1 Gamma ray correlation

Gamma ray profiles for the Staithes S-20 and 42/28-2 boreholes are presented in Figure 3. The correlation used the diagnostic log motifs of lithological units that are known to be persistent over greater distances than the spacing between the two study wells (Bachman et al., 2010). These log motifs are calibrated against core in other wells within the basin. In the Permian Zechstein at the base of 42/28-2, gamma ray values are generally low (~50 API), punctuated by brief peaks to ~200 API. After a final low, gamma ray values increase to ~150 API at the boundary with the Bunter Shale. Only the top of the Zechstein was cored in Staithes S-20. Gamma ray values fall to around ~0 API at ~3,500 ft, corresponding to an interval of bedded halite, before increasing to ~130 API at the base of the Bunter Shale

FIGURE 3
Stratigraphic correlation of the Staithes S-20 and 42/28-2 boreholes based upon gamma ray logs. The wells are vertical, and depths are measured along hole. The Hardegsen Unconformity is marked by the irregular line. A star (*) denotes a palynological age constraint (see Salisbury et al., 2022). Lad−Ladinian, C-N−Carnian-Norian, R−Rhaetian, SSG−Sherwood Sandstone Group, MMG−Mercia Mudstone Group, M−Muschelkalk. Chronology follows Salisbury et al. (2022).

(similar to borehole 42/28-2), enabling correlation between the two boreholes.

Both the Staithes S-20 and 42/28-2 boreholes show relatively stable gamma ray profiles during the lower Bunter Shale (around ~110 API). Gamma ray profiles exhibit a more erratic response during the upper Bunter Shale, beginning at 3,100 ft in Staithes S-20 and ~7,700 ft in borehole 42/28-2. This marks the base of the Rogenstein Member, which includes interbedded sandstones that contribute to the erratic behaviour in gamma ray data. In both records, the boundary between the Bunter Shale and Bunter Sandstone is marked by a sharp upwards decrease in gamma. The Bunter Sandstone exhibits relatively stable but low gamma ray values, around ~60 API, and is particularly distinct in the 42/28-2 borehole record. The Bunter Sandstone terminates with a sharp increase in gamma ray, corresponding to an unconformity at ~2080 ft in Staithes S-20 and ~6,200 ft in 42/28-2. Evidence for a hiatus in sedimentation is observed directly in the core of Staithes S-20

but is only inferred in borehole 42/28-2 based on gamma ray records and regional correlation (Bachman et al., 2010). Throughout the overlying MMG, the gamma ray record is slightly elevated in Staithes S-20. This offset may be a product of different tools or calibration and both records remain relatively stable. Brief lower gamma Mercia Mudstone packages likely mark the position of greater evaporite proportion, as the low potassium content of the rock reduces the background gamma API values.

4.2 Preservation of primary $\delta^{34}S_{evap}$ signals

The precipitation of gypsum is associated with a minor fractionation factor ($\Delta^{34}S_{precipitate-brine}$), with experimental studies reporting a range between +1.6 and +2‰ (Thode and Monster, 1965; Holser and Kaplan, 1966; Nielsen, 1978; Raab and Spiro, 1991; Van Driessche et al., 2016). Although the $\delta^{34}S$ of both the brine and

precipitate decrease progressively with continued evaporation, the results of Raab and Spiro (1991) suggest relatively similar $\Delta^{34}S_{precipitate-brine}$ values are maintained until the middle of the halite stability field. Thus, it is generally assumed that the $\delta^{34}S$ of a marine Ca-sulphate is indicative of the isotopic composition of the brine from which it precipitated (Schreiber and Tabakh, 2000). Considering that we exclusively sampled calcium-sulphates and halite, it is unlikely that changes in mineralogy and/or sulphur isotope reservoir effects associated with prolonged restriction had a major impact on the $\delta^{34}S_{evap}$ records from boreholes 42/28-2 and Staithes S-20.

The $\delta^{34}S_{evap}$ correlation presented in this study is surprising in that the 42/28-2 sediments have been exposed and saturated with drilling fluids: unfortunately, there is no record of what drilling fluids were used when coring. Samples can be fully covered in fluids during the drilling process and washing them away entirely is difficult (Kubo et al., 2016), thus potentially impacting the integrity of sample geochemistry (e.g., Stuckman et al., 2019; Sanei et al., 2020). $\delta^{34}S_{evap}$ values in drill cuttings are vulnerable to contamination by drilling fluids, which can be characterised by a range of different chemical compositions (Ball et al., 2012). However, the similarity between both the Staithes S-20 and 42/28-2 $\delta^{34}S_{evap}$ records in this study would suggest that the drilling fluids used had little to no effect on the sedimentary sulphate. Despite this, future studies should always be aware that the type of drilling fluid used may impact the sulphur isotope record.

Evaporites form in hydrographically isolated marginal marine basins with restricted circulation (Warren, 2010). Local depositional and diagenetic (i.e., post-depositional) processes can alter a global marine $\delta^{34}S_{evap}$ signal recorded in evaporites (Lu et al., 2001; Crockford et al., 2019), potentially limiting the use of $\delta^{34}S_{evap}$ data for stratigraphic correlation. Local effects include riverine inputs of continental sulphate from weathered pyrite and/or evaporites (Lu et al., 2001; Bottrell and Newton, 2006), reservoir effects associated with evaporite precipitation during periods of prolonged restriction (Raab and Spiro, 1991), and microbial sulphur cycling (e.g., microbial sulphate reduction) and subsequent pyrite burial (Bernasconi et al., 2017). Diagenetic effects include syn-sedimentary dissolution/precipitation of halite, the replacement of halite with gypsum (and vice versa) soon after burial (Schreiber and Tabakh, 2000), microbial sulphate reduction below the sediment-water interface (Jorgensen et al., 2019) and a cycle of diagenesis during burial and uplift (Ortí et al., 2022). The latter involves the formation of anhydrite from the dehydration of primary gypsum at moderate to deep burial depths, followed by the rehydration of anhydrite to form secondary gypsum during uplift (Ortí et al., 2022). The sulphur isotopic effect of the dehydration/ rehydration of Ca-sulphates associated with burial and uplift is not well understood. Current evidence suggests it is associated with only minor sulphur isotope fractionation (see Ortí et al., 2022 for details), and is unlikely to have imparted any major effect on our $\delta^{34}S_{evap}$ records. During burial to temperatures exceeding 120°C, thermochemical sulphate reduction can occur, involving the chemical reduction of sulphate to sulphide, and the sulphurisation of organic matter (see review by Cai et al., 2022). This process has been associated with significant sulphur isotope fractionations in metal sulphide deposits (Cai et al., 2022). However, only a minor degree of sulphur isotope fractionation occurs between

sulphate and sulphide in most petroleum-related sour gas settings (Worden et al., 1997; Cai et al., 2022), likely due to the complete reduction of any anhydrite that dissolves, with sulphate dissolution being rate limiting (Meshoulum et al., 2016; Cai et al., 2022).
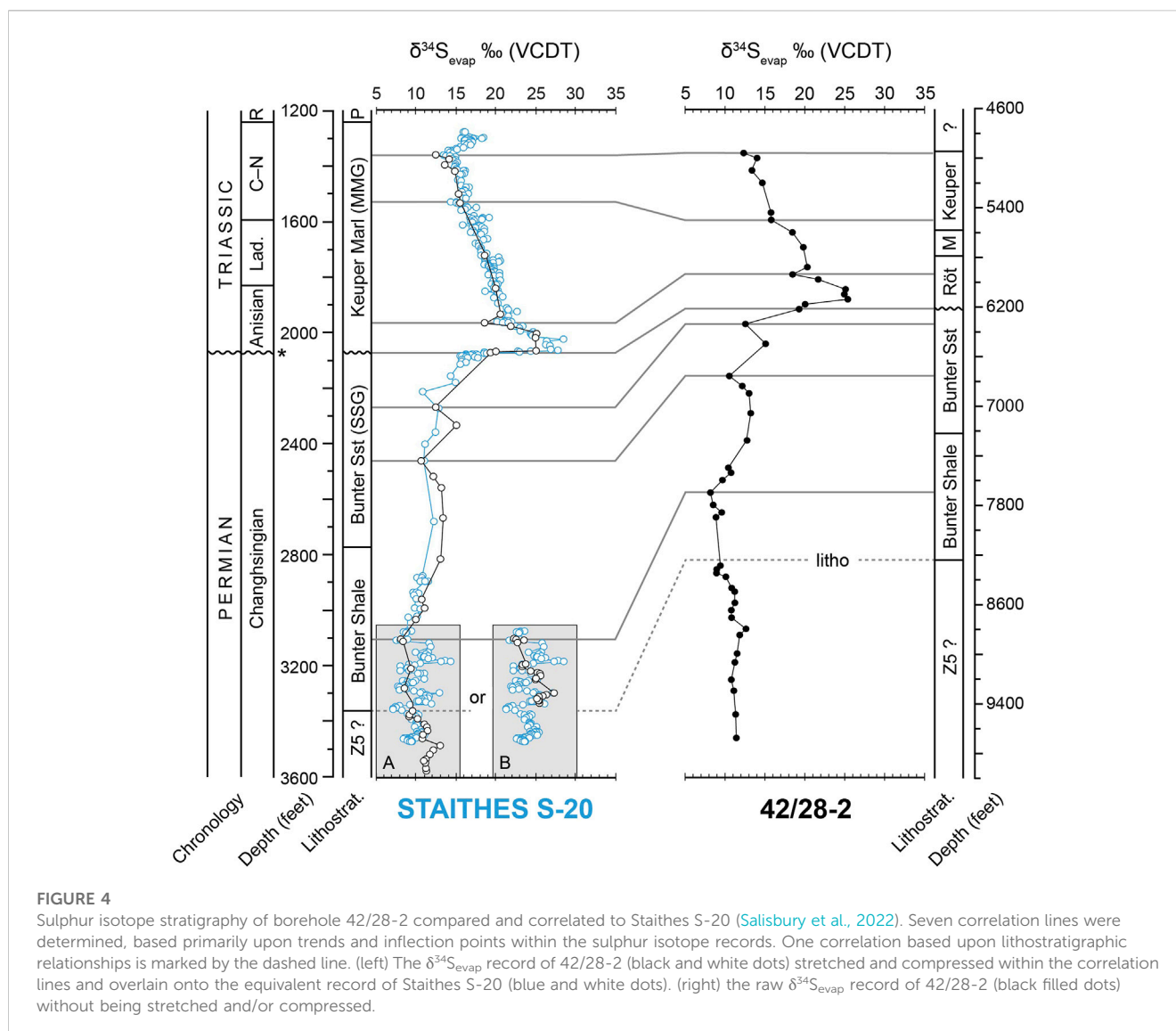
It is understood that diagenetic fluids exhibit a high degree of spatial isotopic heterogeneity and will produce more scattered $\delta^{34}S$ values in rocks that have interacted with diagenetic fluids, limiting the stratigraphic reproducibility of $\delta^{34}S_{evap}$ records between different basins (Metzger et al., 2014). Thus, a high degree of stratigraphic reproducibility in $\delta^{34}S$ is generally considered to be evidence of a global isotopic signal (Metzger et al., 2014). The $\delta^{34}S_{evap}$ curve from Staithes S-20 has been shown to represent a global record of marine sulphate (Salisbury et al., 2022). The small degree of scatter and/or minor offsets between the $\delta^{34}S_{evap}$ curves of Staithes S-20 and 42/28-2 may reflect local depositional and minor diagenetic effects, but the robust correlation between them (Figure 4), as well as their agreement with the global $\delta^{34}S_{evap}$ record (Salisbury et al., 2022), suggest that the long-term trends in the $\delta^{34}S_{evap}$ data represent a global marine sulphur isotope signal.

4.3 Sulphur isotope correlation

The $\delta^{34}S_{evap}$ record from borehole 42/28-2 is presented alongside Staithes S-20 (Salisbury et al., 2022) in Figure 4. Clear stratigraphic trends are apparent in both $\delta^{34}S_{evap}$ records even at different sample resolutions. The principles of sulphur isotope stratigraphy and isotope correlation are based on; (1) the assumption that the sulphur isotope composition of the ocean is isotopically homogenous at any given time, and hence, the absolute $\delta^{34}S_{evap}$ value; (2) the trend in the $\delta^{34}S_{evap}$ is directly comparable (i.e., positive versus negative); and (3) inflection points in $\delta^{34}S_{evap}$ represent a shift from one slope to another. It would be appealing to correlate all the trends and inflections points in Figure 4, however, caution needs to be exercised due to the different sampling resolution between the boreholes. Thus, in Figure 4 we have only chosen to correlate seven points through the latest Permian to Late Triassic time interval. In addition, we have chosen to use one lithostratigraphic correlation which will be discussed below.

During the correlation process between borehole 42/28-2 and Staithes S-20, the stratigraphy is assumed to be proportionally equivalent and each stratigraphic element (apart from truncation by the unconformity) is assumed to expand or contract at a similar rate (see left-hand side Figure 4). If a comparable sample resolution was obtained for borehole 42/28-2, then the correlation between the boreholes (core versus cuttings) would have been stronger. However, this was not possible due to the stratigraphic resolution of the drill cuttings collected and the fact that many cutting samples did not contain any evaporitic minerals for isotopic analysis. Similar concerns (e.g., stratigraphic thickness and time, as well as sample resolution) were highlighted by Gröcke (2020) when performing carbon isotope stratigraphy for correlation. The same issues apply for all types of correlation using isotope stratigraphy.

Cyclic variability in $\delta^{34}S_{evap}$ is observed through the Zechstein and lower Bunter Shale intervals in Staithes S-20 (3,100–3,500 ft: Figure 4). This apparent cyclicity is not observed in the equivalent interval of borehole 42/28-2 (7,700–9,680 ft), although this may be in part due to lower sample resolution (Figures 4A,B). If the cyclicity

FIGURE 4
Sulphur isotope stratigraphy of borehole 42/28-2 compared and correlated to Staithes S-20 (Salisbury et al., 2022). Seven correlation lines were determined, based primarily upon trends and inflection points within the sulphur isotope records. One correlation based upon lithostratigraphic relationships is marked by the dashed line. (left) The $\delta^{34}S_{evap}$ record of 42/28-2 (black and white dots) stretched and compressed within the correlation lines and overlain onto the equivalent record of Staithes S-20 (blue and white dots). (right) the raw $\delta^{34}S_{evap}$ record of 42/28-2 (black filled dots) without being stretched and/or compressed.

observed in Staithes S-20 reflects global changes in the sulphate isotopic reservoir, then the cycles may prove very useful in high-resolution correlation of the Zechstein throughout Europe. Future sulphur isotope studies of the Zechstein should be performed at high resolution to assess reproducibility of the apparent cyclicity observed in Staithes S-20. After this period of cyclicity, $\delta^{34}S_{evap}$ gradually increases throughout the Bunter Shale and Bunter Sandstone from approximately +8‰ to +15‰ in both boreholes. This range in $\delta^{34}S_{evap}$ constrains the age of these stratigraphic units to the latest Permian (Claypool et al., 1980; Crockford et al., 2019; Present et al., 2020; Salisbury et al., 2022), suggesting the placement of the PTB in this part of the Southern Permian Basin should be shifted from the upper boundary of the Zechstein evaporites to a point within the Bunter Sandstone (Figure 5). This is significant, due to its' apparent conflict with biostratigraphic constraints for an Early to Middle Triassic age for Bunter Sandstone equivalents in southern England and Germany (see above). Although, this part of the record is more difficult to accurately correlate based on principles (2) and (3) described above, a late Permian age for the lower Bunter in the

SNS Basin suggests that towards the basin margins, the Bunter stratigraphic motif is aliased by an older continental clastic system. By extension, it is also possible that the lower parts of the onshore Sherwood Sandstone Group in northern England also extend into the late Permian.

Due to erosion associated with the Hardegsen unconformity in the Early Triassic (Bachman et al., 2010), the $\delta^{34}S_{evap}$ curves of Staithes S-20 and 42/28-2 fail to record the large positive $\delta^{34}S_{evap}$ excursion characteristic of the Early Triassic. The entire evaporite-based stratigraphic interval of the Staithes S-20 borehole hinges on the constraint of a single palynological age (earliest Anisian), which is obtained from immediately above the unconformity (see Salisbury et al., 2022). $\delta^{34}S_{evap}$ values of > +15‰ above the unconformity in Staithes S-20 also support an Anisian age when compared with the global composite record as discussed in Salisbury et al. (2022). Based on absolute $\delta^{34}S_{evap}$ values at this point it is evident that borehole 42/28-2 records the Anisian recovery to pre-excursion $\delta^{34}S_{evap}$ values in the Olenekian that persisted prior to the negative excursion (Figure 4). $\delta^{34}S_{evap}$ values in borehole 42/28-2 show a
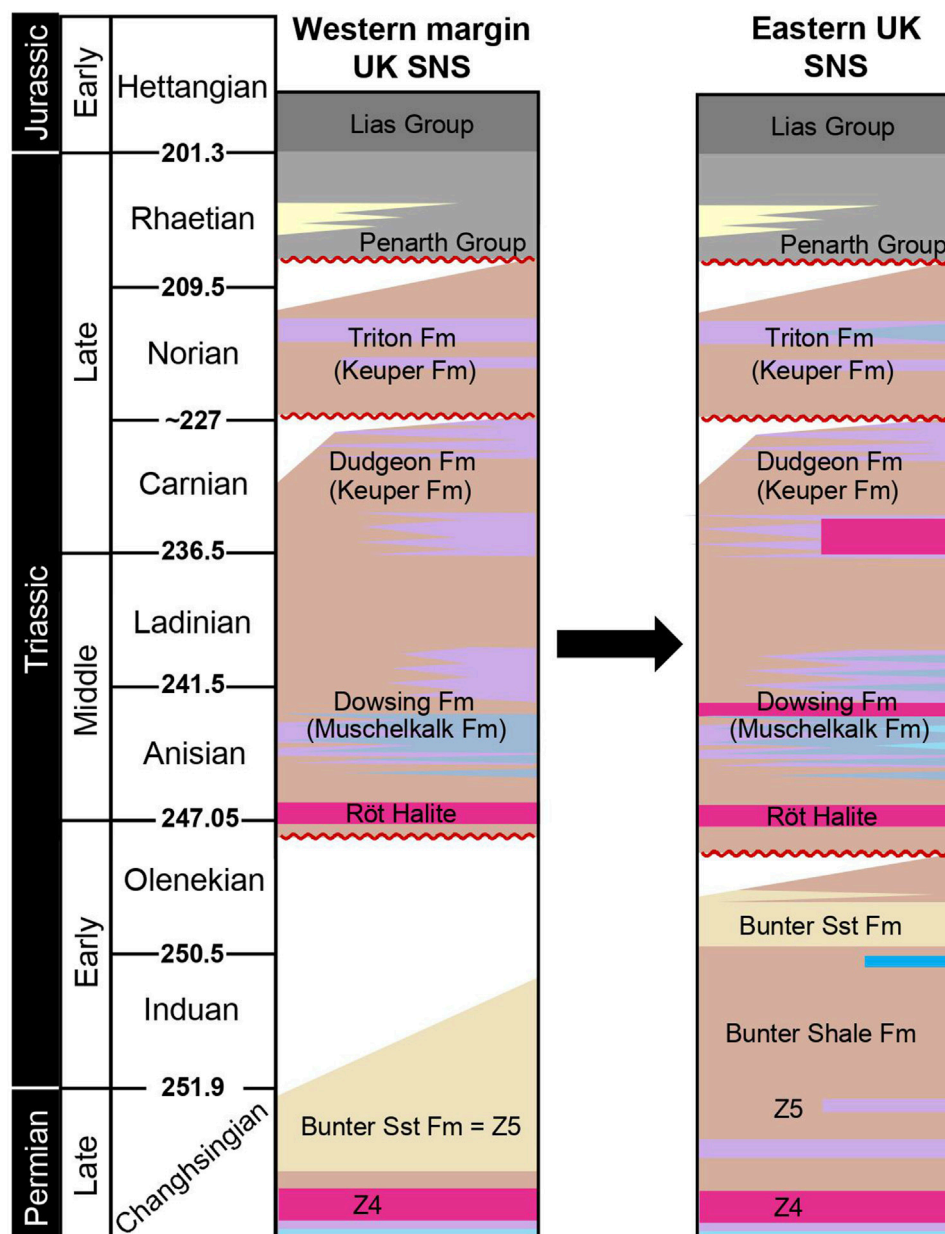
FIGURE 5
Revised lithostratigraphic framework for the western margin UK Southern North Sea (SNS) compared with the established lithostratigraphy of the eastern UK SNS. Unconformities are marked with red irregular lines.

declining trend, similar to that which is recorded in Staithes S-20, for the remainder of the Triassic—ending with $\delta^{34}S_{evap}$ values of ~ +12‰ in the Norian.

As shown in Figure 4 the correlation is somewhat more uncertain when there are larger gaps in the $\delta^{34}S_{evap}$ record (e.g., Bunter Sandstone) from borehole 42/28-2. This is to be expected, as lower resolution records will fail to capture the full extent of isotopic variability (especially short-term changes), creating the false impression of greater isotopic heterogeneity between sedimentary basins (Metzger et al., 2014). It is thus unclear whether the lack of cyclicity at the base of 42/28-2 (discussed above) reflects a difference in the evolution of the sulphur cycle between the Cleveland and

southern North Sea basins during this time interval. We present two potential correlations (see Figures 4A,B) between Staithes S-20 and borehole 42/28-2 during the latest Permian. Figure 4A assumes that the lithostratigraphic boundary between Z5 and the Bunter Shale is age equivalent in both boreholes (dashed correlation line). In contrast, Figure 4B displays a correlation scheme based entirely upon the $\delta^{34}S_{evap}$ data, thus suggesting a different age for the boundary between Z5 and the Bunter Shale in each borehole, taking account of the possible diachroneity of lithostratigraphic boundaries. Each of these correlations are plausible but highlight the issue when performing sulphur isotope correlation during time intervals with little isotopic variability (akin to strontium isotope
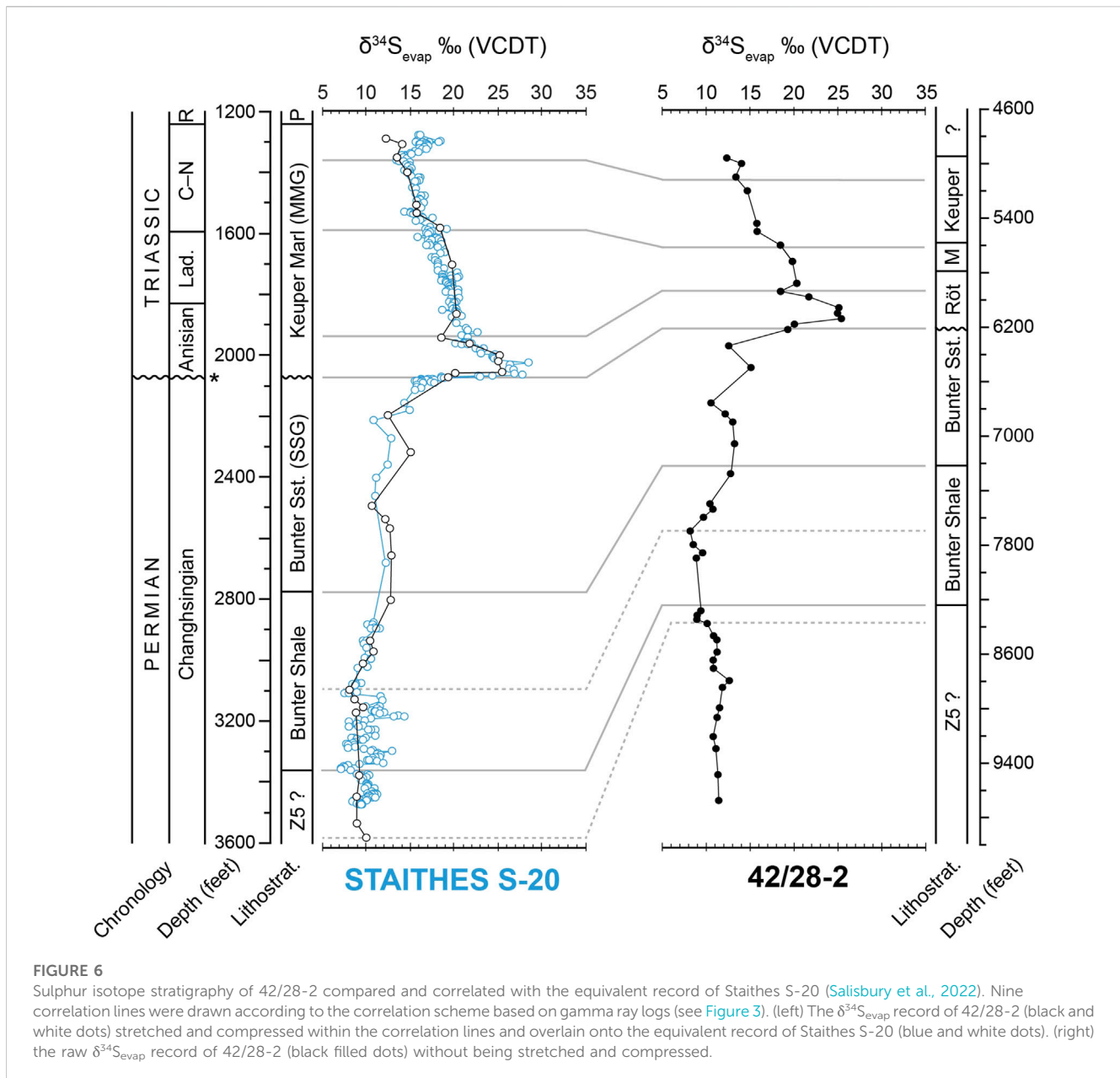
FIGURE 6
Sulphur isotope stratigraphy of 42/28-2 compared and correlated with the equivalent record of Staithes S-20 (Salisbury et al., 2022). Nine correlation lines were drawn according to the correlation scheme based on gamma ray logs (see Figure 3). (left) The $\delta^{34}S_{evap}$ record of 42/28-2 (black and white dots) stretched and compressed within the correlation lines and overlain onto the equivalent record of Staithes S-20 (blue and white dots). (right) the raw $\delta^{34}S_{evap}$ record of 42/28-2 (black filled dots) without being stretched and compressed.

stratigraphy). Additional techniques such as evaporite palynology (Gibson & Wellman, 2021) may help to constrain age and sulphur isotope correlation during the late Permian Zechstein. Despite this, the correlation between 42/28-2 and Staithes S-20 looks exceptionally good, even with different sampling resolutions.

It should be noted that data resolution is not the only factor to consider when attempting to derive robust, high-resolution isotope stratigraphic correlations. As briefly discussed above, the rate and magnitude of sulphur isotope variability are of crucial importance (see Yao et al., 2019). Between the depths of 6,760 ft and 5,940 ft in the borehole 42/28-2 dataset, robust correlations can be achieved with the Staithes S-20 record, despite the relatively low sample resolution of 42/28-2. This is due to the abrupt and significant shift in the $\delta^{34}S_{evap}$ record during this depth interval (see Figure 4), which is also reflected in the global $\delta^{34}S_{evap}$ curve (see Salisbury et al., 2022). Therefore, if the time-interval studied exhibits high sulphur isotopic

variability, a sample resolution comparable to our Staithes S-20 record may not be essential. This study has thus demonstrated that drill cuttings can be confidently used for $\delta^{34}S_{evap}$ stratigraphic correlation of sedimentary sequences between sedimentary basins.

4.4 Wireline log-based lithostratigraphy versus $\delta^{34}S_{evap}$ correlation

To compare the gamma ray and sulphur isotope correlations, we used the gamma ray correlation lines shown in Figure 3 to correlate the $\delta^{34}S_{evap}$ curves from Staithes S-20 and borehole 42/28-2 (Figure 6). Seven confident gamma ray motifs were correlated based on their visual similarity. An additional gamma ray correlation was tentatively assigned in the middle Bunter Shale (see Figure 3, dashed line) at the shift from moderate scatter to
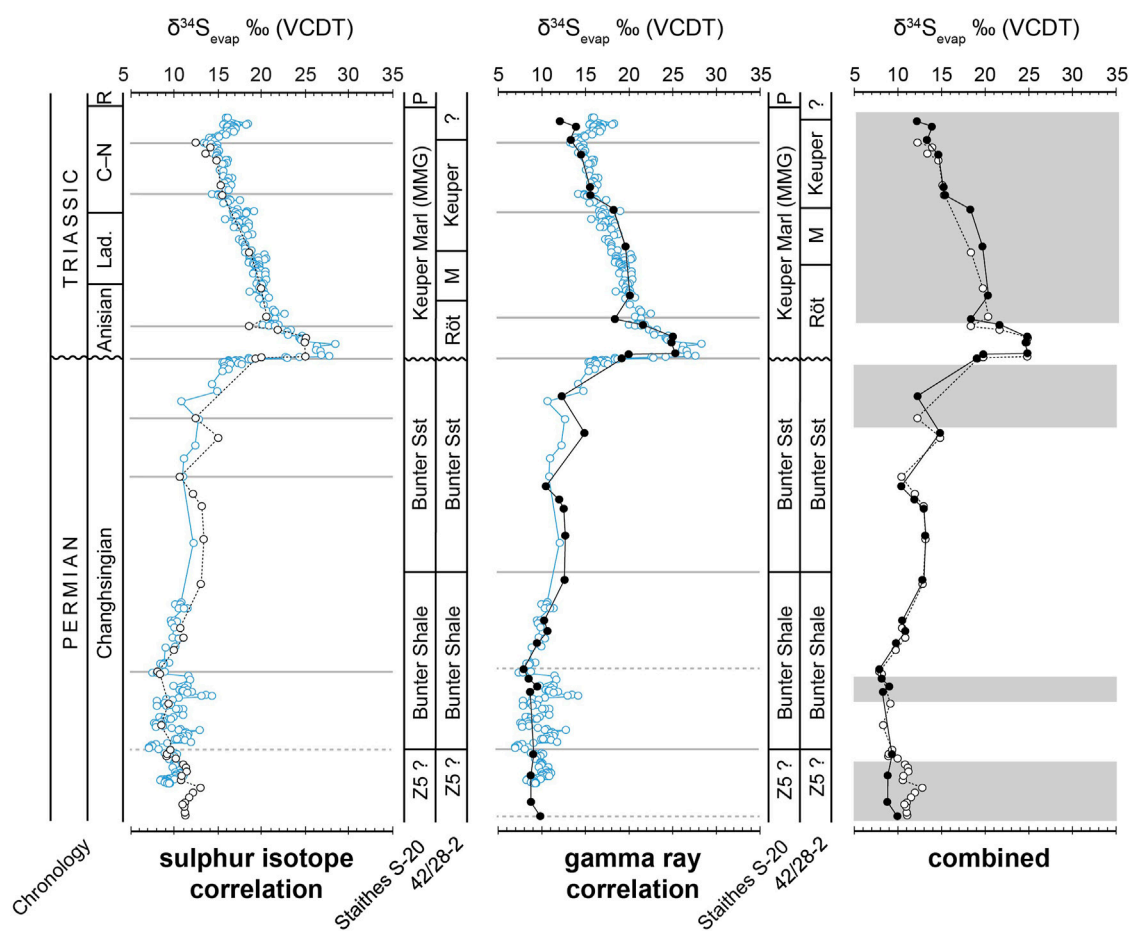
FIGURE 7
Comparison between the sulphur isotope and gamma ray correlation schemes. (left) Stratigraphic correlation based upon the sulphur isotope records, as presented in Figure 4. The lithostratigraphic boundaries for Staithes S-20 are based on the original log, while those for 42/28-2 are adjusted based upon the correlation schemes with Staithes S-20. (middle) The correlation scheme based upon the gamma ray logs. (right) The $\delta^{34}S_{evap}$ record of Staithes S-20 and 42/28-2 based on the sulphur isotope and gamma ray correlation schemes. Stratigraphic intervals within which the correlation schemes are in relative agreement are marked with the white shading, while the grey shading represents stratigraphic intervals within which the correlation schemes disagree.

high scatter in the record. Based on these correlation lines, the $\delta^{34}S_{evap}$ curves are also strikingly similar, however, there are some key differences. For example, based on gamma ray correlation, borehole 42/28-2 extends further back in time in Zechstein cycle Z5. Thus, using gamma ray stratigraphy only the top 4 samples in Z5 from borehole 42/48-2 correlate with the Staithes S-20 $\delta^{34}S_{evap}$ record (Figure 6).

Another key difference is in the correlation of the Röt Halite Member (Triassic). Gamma ray correlation would erroneously imply that the Röt Halite Member extends into the Ladinian, whilst the sulphur isotope correlation constrains it to the Anisian (Figure 7). It is plausible this may reflect errors in the application of lithostratigraphy during the original logging process. In the case of the Staithes S-20 borehole, the lack of clear halite intervals defining both the Röt and Muschelkalk halites, and the facies transition from the limestone-prone Muschelkalk into clastic basin margin facies, has made the log motifs ambiguous. This demonstrates how $\delta^{34}S_{evap}$ records provide a critical constraint on the validity of lithostratigraphy for stratigraphic correlation, particularly where

the lithostratigraphic data exhibit greater ambiguity, such as basin margin settings.

Published data provide further contrasting age estimates. Previous lithostratigraphic correlations suggest an Olenekian age for the Röt Halite Member (Warrington et al., 1980), while more recent work suggests an early Anisian age, in broad agreement with our $\delta^{34}S_{evap}$ record (Bachmann et al., 2010). Isotopic analysis of fluid inclusions suggests a late Early Triassic age for the Röt in the Netherlands, Germany and Poland, reporting $\delta^{34}S$ values between +27.1‰ and +32‰ (Kovalevych et al., 2002). In contrast, we only record $\delta^{34}S_{evap}$ values between +18.5‰ and +25.4‰ (Figure 4). The reason for this difference is currently unclear, however, it should be noted that Kovalevych et al. (2002) used a different analytical method for sulphur isotope analysis (e.g., offline SO_2 generation versus online continuous flow IRMS at SIBL). Furthermore, the Röt may have formed earlier to the east of the UK and SNS. Additional sulphur isotope analyses of the Röt Halite Member are required to constrain its' age and determine if this lithostratigraphic unit is diachronous or synchronous across basins.

Correlations using gamma ray and $\delta^{34}S_{evap}$ data suggest that the successions in each well are broadly comparable across the Cleveland and SNS basins (Figure 7). This can be clearly seen in the Anisian interval (Figure 7). The position of the Hardegsen unconformity can be located using the gamma ray logs (Figure 3) and the Anisian exhibits a high rate and magnitude of sulphur isotopic variability (Figure 4), enabling a robust correlation to be made. Interestingly, the correlation schemes exhibit greatest disagreement during the Ladinian, Carnian and Norian (Figure 7). In particular, the sulphur isotope correlation suggests the top of the Mercia Mudstone in borehole 42/28-2 extends into the Carnian–Norian, while the gamma ray correlation suggests it extends until just below the Norian–Rhaetian boundary, possibly reflecting issues with depth averaging between the gamma ray and $\delta^{34}S_{evap}$ records. In this case the sulphur isotope correlation scheme would be favoured, demonstrating the capacity for sulphur isotope stratigraphy to capture lithofacies diachroneity.

The $\delta^{34}S_{evap}$ correlation based on gamma ray is quite robust but has limitations when compared to the sulphur isotope correlation, which is independent of lithostratigraphy (Figure 7). Due to the 'layer cake' appearance of the Triassic southern North Sea, lithostratigraphy assumes that the deposition of one facies is "time-equivalent" to the same facies in another basin. When using gamma ray to correlate $\delta^{34}S_{evap}$ one is forcing it to fit in line with the principles of lithostratigraphy. The deposition of an evaporite in one basin may not be time equivalent to the deposition of an evaporite in a nearby basin, and hence, wireline log correlations of apparently similar log motifs could cross time boundaries. The stability and residence time of sulphur in the ocean precludes crossing time boundaries as at any given time the ocean will have a homogenous $\delta^{34}S_{evap}$ signature (Paytan et al., 2012). Therefore, as time changes, so will the $\delta^{34}S_{evap}$ signature of the ocean. In Figure 6 it is assumed that the gamma ray correlation is a timeline and hence, only four $\delta^{34}S_{evap}$ data from borehole 42/28-2 are correlatable to the Staithes S-20 record for the Z5 lithology (see Figure 4A). However, if we consider that the Z5 evaporite sequence in borehole 42/28-2 is "time-equivalent" to the base of the Bunter Shale in the Staithes S-20 core/basin, then this would create a very different correlation curve (see Figure 4B). Thus, a significant strength of sulphur isotope stratigraphy is that it provides independent validation on whether straight lithostratigraphic correlations are accurate, differentiating between log motifs that appear similar but represent strata of distinct ages.

The above discussion reflects the importance of sample resolution and isotopic variability in deriving robust stratigraphic correlations (see Yao et al., 2019 for further discussion). The $\delta^{34}S_{evap}$ data from the Zechstein and the base of the Bunter Shale lack the sample resolution and isotopic variability to facilitate high-resolution correlations. In contrast, although the sample resolution is comparable in the Mercia Mudstone Group, the greater isotopic variability enables high-resolution correlations to be made using $\delta^{34}S_{evap}$ alone (Figures 4, 7). For intervals where high sampling resolution cannot be achieved, or where the $\delta^{34}S$ record exhibits relative stability through time, we suggest a multidisciplinary approach, integrated with wireline log stratigraphy, to produce a global $\delta^{34}S$ evaporite curve for correlation. With further research, it is anticipated that the $\delta^{34}S$

curve from evaporites may become comparable to how strontium isotope stratigraphy is used for global correlation of marine sediments. More importantly, placing evaporite-bearing strata into more constrained stratigraphic timelines will increase our knowledge of these extreme environments in Earth's history.

4.5 Implications for carbon capture and storage

As discussed, our $\delta^{34}S_{evap}$ records from the Staithes S-20 and 42/28-2 boreholes provide further chronostratigraphic constraint for the late Permian–Triassic strata of the Cleveland and UK SNS basins. In particular, the base of the Bunter Sandstone has been assigned to the latest Permian, suggesting the PTB may occur within the Bunter Sandstone at these locations (Figure 5). This enables the degree of Hardegsen erosion to be better constrained stratigraphically (i.e., when it initiated and stopped in a basin). This will help to develop more accurate palaeogeographic maps for the latest Permian and Triassic of the United Kingdom. This is of particular significance due to the interest in the Bunter Sandstone as a potential reservoir for carbon capture and storage (CCS) (Holloway et al., 2006; Newell and Shariatipour, 2016; Alshakri et al., 2023, *in press*).

The use of geological reservoirs for the storage of sequestered carbon dioxide (CO_2) as a super-critical fluid is thought to be a key technology for addressing anthropogenic climate change (Bickle, 2009). The Bunter Sandstone and other equivalents within the Sherwood Sandstone Group are considered suitable candidates for CO_2 storage (Brook et al., 2003; Holloway et al., 2006). This is due to the Bunter Sandstone's favourable reservoir properties (Chadwick et al., 2008; Dobbs et al., 2018), with fair to good porosity and permeability (Noy et al., 2012), and suitable stratigraphic position, whereby it is sealed by a durable caprock, the overlying saliferous Mercia Mudstone Group (Armitage et al., 2013). In addition, its supposed sheet-like geometry is predicted to be conducive to effective pressure dissipation and reliable injectivity.

It should be noted, however, that an accurate understanding of the regional stratigraphic framework is essential for reliably estimating the suitability of a reservoir for CO_2 storage. For example, the spatial variability in properties (Ringrose, 2020) such as sand:shale ratios, porosity, and permeability within the Bunter Sandstone can be mapped for assessing its' suitability for CO_2 storage. These assessments are likely erroneous if our revised stratigraphic framework for the western margin SNS is correct, as authors of previous research will have contoured the properties from sandstones of different ages. In addition, although drillcore can provide useful insights, it is common for analogous facies to be studied at outcrop to provide a broader view of the heterogeneities present within reservoir zones (e.g., Newell and Shariatipour, 2016). However, such studies commonly focus on the onshore Sherwood Sandstone outcrops, which were deposited by large river systems during the Early Triassic, a time interval characterised by a warmer and wetter climate than the late Permian (Trotter et al., 2015). Thus, if the base of the Bunter Sandstone in the western margin SNS is truly latest Permian in age then the depositing rivers would have experienced lower volume discharges leading to

different reservoir architectures and heterogeneities (Issautier et al., 2014). As a result, alternative analogue facies may need to be found from more ephemeral fluvial systems. These issues will impact the reliability of dynamic models used to predict the outcome of different scenarios, such as injection rates, well counts and locations (e.g., Noy et al., 2012; Williams et al., 2013; Tucker, 2018; Ringrose, 2020). This could lead to suboptimal developments, financial implications and a potential to fail contractual obligations.

5 Conclusion

Sulphur isotope stratigraphy using evaporites has the potential to enhance chronostratigraphic constraints for Permian–Triassic strata of the United Kingdom and continental Europe. Unfortunately, complete drill cores are uncommon and thus, determining whether drill cuttings are suitable for constructing $\delta^{34}S_{evap}$ records is essential. A $\delta^{34}S_{evap}$ record was produced from drill cuttings of borehole 42/28-2 in the southern North Sea basin. This $\delta^{34}S_{evap}$ record was compared to the onshore Staithes S-20 borehole. Our findings show that $\delta^{34}S_{evap}$ records derived from drill cuttings can be used for stratigraphic correlation, although we advise that during periods of relative stability in $\delta^{34}S_{evap}$ a multidisciplinary approach is adopted (i.e., coupled with gamma ray stratigraphy). Based on our $\delta^{34}S_{evap}$ records between the Cleveland Basin and southern North Sea Basin in this study, the deposition of the Bunter Shale and Bunter Sandstone is determined to have initiated in the latest Permian, while the youngest age of the MMG is Anisian (Middle Triassic). Neither $\delta^{34}S_{evap}$ curves record the Early Triassic due to erosion associated with the Hardegsen unconformity. Our findings thus suggest that the PTB should be defined somewhere within the Bunter Sandstone, and not at the upper boundary of the Zechstein evaporites in the Cleveland and Southern North Sea basins. This implies that our current understanding of the regional lithostratigraphy is likely overly simplistic and fails to capture the full extent of facies diachroneity, particularly on the basin margins. This is especially noteworthy for the Bunter Sandstone, due to interest in its' possible suitability as a reservoir for CO_2 storage in the United Kingdom.

Data availability statement

The original contributions presented in the study are included in the article/Supplementary Material, further inquiries can be directed to the corresponding authors.

Author contributions

DRG and JS conceptualized the study. JS carried out the chemical sample preparation, as well as the isotopic analyses under the supervision of DRG. JS wrote the manuscript with contributions from DRG and TM. All authors contributed to the article and approved the submitted version.

Conflict of interest

The author TM was employed by Shell UK Exploration and Production.

The remaining authors declare that the research was conducted in the absence of any commercial or financial relationships that could be construed as a potential conflict of interest

Publisher's note

All claims expressed in this article are solely those of the authors and do not necessarily represent those of their affiliated organizations, or those of the publisher, the editors and the reviewers. Any product that may be evaluated in this article, or claim that may be made by its manufacturer, is not guaranteed or endorsed by the publisher.

Supplementary material

The Supplementary Material for this article can be found online at: https://www.frontiersin.org/articles/10.3389/feart.2023.1216365/full#supplementary-material

References

Alshakri, J., Hampson, G. J., Jaquemyn, C., Jackson, M., Petrovskyy, D., Geiger, S., et al. (2023). "A screening assessment of the impact of sedimentological heterogeneity on CO_2 migration and stratigraphic-baffling potential: Sherwood and Bunter Sandstones, UK," in *Enabling secure subsurface storage in future energy systems*. Editors J. M. Miocic, N. Heinemann, K. Edlmann, J. Alcade, and R. A. Schultz (Nottingham: Geological Society of London Special Publications). doi:10.1144/SP528-2022-34

Ambrose, K., Hough, E., Smith, N. J. P., and Warrington, G. (2014). *Lithostratigraphy of the Sherwood Sandstone Group of England, Wales and south-west Scotland*. Nottingham: British Geological Survey Research Report. *RR/14/01*.

Ambrose, K., and Wakefield, O. (2015). Permo-Triassic rocks of Nottingham. *Mercian Geol.* 18, 260–263.

Armitage, P. J., Worden, R. H., Faulkner, D. R., Aplin, A. C., Butcher, A. R., and Espie, A. A. (2013). Mercia Mudstone Formation caprock to carbon capture and storage sites: Petrology and petrophysical characteristics. *J. Geol. Soc.* 170, 119–132. doi:10.1144/jgs2012-049

Bachman, G. H., Geluk, M. C., Warrington, G., Becker-Roman, A., Beutler, G., Hagdorn, H., et al. (2010). "Triassic," in *Petroleum geological atlas of the Southern Permian Basin area*. Editors J. C. Doornenbal and A. G. Stevenson (Houten: EAGE Publications), 149–173.

Bachman, G. H., and Kozur, H. W. (2004). The Germanic Triassic: Correlations with the international chronostratigraphic scale, numerical ages and Milankovitch cyclicity. *Hallesches Jahrb. geowiss.* 26, 17–62. doi:10.25673/91844

Ball, A. S., Stewart, R. J., and Schliephake, K. (2012). A review of the current options for the treatment and safe disposal of drill cuttings. *Waste Manag. Res.* 30 (5), 457–473. doi:10.1177/0734242X11419892

Bernasconi, S. M., Meier, I., Wohlwend, S., Brack, P., Hochuli, P. A., Bläsi, H., et al. (2017). An evaporite-based high-resolution sulfur isotope record of Late Permian and Triassic seawater sulfate. *Geochim. Cosmochim. Acta* 204, 331–349. doi:10.1016/j.gca.2017.01.047

Bickle, M. J. (2009). Geological carbon storage. *Nat. Geosci.* 2, 815–818. doi:10.1038/ngeo687

Boschetti, T., Cortecci, G., Toscani, L., and Iacumin, P. (2011). Sulfur and oxygen isotopic compositions of Upper Triassic sulfates from northern Apennines (Italy): Paleogeographic and hydrogeochemical implications. *Geol. Acta* 9, 129–147.

Bottrell, S. H., and Newton, R. J. (2006). Reconstruction of changes in global sulfur cycling from marine sulfate isotopes. *Earth Sci. Rev.* 75, 59–83. doi:10.1016/j.earscirev.2005.10.004

Brook, M., Shaw, K., Vincent, C., and Holloway, S. (2003). *Storage potential of the Bunter Sandstone in the UK sector of the southern North Sea and the adjacent onshore area of Eastern England*. Nottingham: British Geological Survey Commissioned Report, 37. CR/03/154.

Bryant, R. N., Present, T. M., Ahm, A-S. C., McClelland, H-L. O., Razionale, D., and Blättler, C. L. (2022). Early diagenetic constraints on Permian seawater chemistry from the Capitan Reef. *Geochim. Cosmochim. Acta* 328, 1–18. doi:10.1016/j.gca.2022.04.027

Cai, C., Li, H., Li, K., and Wang, D. (2022). Thermochemical sulfate reduction in sedimentary basins and beyond: A review. *Chem. Geol.* 607, 121018. doi:10.1016/j.chemgeo.2022.121018

Cao, H., Kaufman, A. J., Shan, X., Cui, H., and Zhang, G. (2016). Sulfur isotope constraints on marine transgression in the lacustrine Upper Cretaceous Songliao Basin, northeastern China. *Palaeogeogr. Palaeoclimatol. Palaeoecol.* 451, 152–163. doi:10.1016/j.palaeo.2016.02.041

Chadwick, R. A., Arts, R., Bernstone, C., May, F., Thibeau, S., and Zweigel, P. (2008). *Best practice for the storage of CO₂ in saline aquifers*, British Geological Society Special Publication No. 14. Nottingham: British Geological Society, 1–267.

Chen, Y., Scholze, F., Richoz, S., and Zhang, Z. (2017). Middle Triassic conodont assemblages from the Germanic Basin: Implications for multi-element taxonomy and biogeography. *J. Syst. Palaeontol.* 17, 359–377. doi:10.1080/14772019.2018.1424260

Claypool, G. E., Holser, W. T., Kaplan, I. R., Sakai, H., and Zak, I. (1980). The age curves of sulfur and oxygen isotopes in marine sulfate and their mutual interpretation. *Chem. Geol.* 28, 199–260. doi:10.1016/0009-2541(80)90047-9

Crockford, P. W., Kunzmann, M., Bekker, A., Hayles, J., Bao, H., Halverson, G. P., et al. (2019). Claypool continued: Extending the isotopic record of sedimentary sulfate. *Chem. Geol.* 513, 200–225. doi:10.1016/j.chemgeo.2019.02.030

Dobbs, M. R., Cuss, R. J., Ougier-Simonin, A., Parkes, D., and Graham, C. C. (2018). Yield envelope assessment as a preliminary screening tool to determine carbon capture and storage viability in depleted southern north-sea hydrocarbon reservoirs. *Int. J. Rock Mech. Min. Sci.* 102, 15–27. doi:10.1016/j.ijrmms.2017.11.018

Eldrett, J. S., Vieira, M., Gallagher, L., Hampton, M., Blaauw, M., and Swart, P. K. (2021). Late Cretaceous to Palaeogene carbon isotope, calcareous nannofossil and foraminifera stratigraphy of the Chalk Group, Central North Sea. *Mar. Pet. Geol.* 124, 104789. doi:10.1016/j.marpetgeo.2020.104789

Franz, M., Henniger, M., and Barnasch, J. (2013). The strong diachronous Muschelkalk/Keuper facies shift in the Central European basin: Implications from the type-section of the Erfurt Formation (Lower Keuper, Triassic) and basin-wide correlations. *Int. J. Earth Sci.* 102, 761–780. doi:10.1007/s00531-012-0823-y

Gallois, R. W. (2009). The lithostratigraphy of the Penarth Group (Late Triassic) of the Severn Estuary area. *Geoscience South-West Engl.* 12, 71–84.

Geluk, M., McKie, T., and Kilhams, B. (2018). "An introduction to the Triassic: Current insights into the regional setting and energy resource potential of NW Europe," in *Mesozoic resource potential in the Southern Permian Basin*. Editors B. Kilhams, P. A. Kukla, S. Mazur, T. McKie, H. F. Mijnlieff, and K. van Ojik (London: Geological Society, London, Special Publications) 469, 139–147. doi:10.1144/SP469

Gibson, M. E., and Wellman, C. H. (2021). The use of spore-pollen assemblages to reconstruct vegetation changes in the Permian (Lopingian) Zechstein deposits of northeast England. *Rev. Palaeobot. Palynol.* 288, 104399. doi:10.1016/j.revpalbo.2021.104399

Gröcke, D. R. (2020). "Carbon isotope stratigraphy: Principles and applications". in *Stratigraphy and Timescales*. Editor M. Montenari (London: Elsevier Academic Press), 5, 1–40. doi:10.1016/bs.sats.2020.08.002

He, T., Dal Corso, J., Newton, R. J., Wignall, P. B., Mills, B. J. W., Todaro, S., et al. (2020). An enormous sulfur isotope excursion indicates marine anoxia during the end-Triassic mass extinction. *Sci. Adv.* 6, eabb6704. doi:10.1126/sciadv.abb6704

He, T., Zhu, M., Mills, B. J. W., Wynn, P. M., Zhuravlev, A. Y., Tostevin, R., et al. (2019). Possible links between extreme oxygen perturbations and the Cambrian radiation of animals. *Nat. Geosci.* 12, 468–474. doi:10.1038/s41561-019-0357-z

Holloway, S., Milodowski, A. E., Strong, G. E., and Warrington, G. (1989). The Sherwood Sandstone Group (Triassic) of the Wessex Basin, southern England. *Proc. Geol. Assoc.* 100, 383–394. doi:10.1016/S0016-7878(89)80056-2

Holloway, S., Vincent, C. J., and Kirk, K. L. (2006). Industrial carbon dioxide emissions and carbon dioxide storage potential in the UK. Nottingham: British Geological Survey Commercial Report. CR/06/185.

Holser, W. T., and Kaplan, I. R. (1966). Isotope geochemistry of sedimentary sulfates. *Chem. Geol.* 1, 93–135. doi:10.1016/0009-2541(66)90011-8

Horacek, M., Brandner, R., Richoz, S., and Povoden-Karadeniz, E. (2010). Lower Triassic sulphur isotope curve of marine sulphates from the Dolomites, N-Italy. *Palaeogeogr. Palaeoclimatol. Palaeoecol.* 290, 65–70. doi:10.1016/j.palaeo.2010.02.016

Hounslow, M. W., and Ruffell, A. H. (2006). "Triassic: Seasonal rivers, dusty deserts and saline lakes," in *The Geology of England and Wales*. Editors P. F. Rawson and P. Brenchley (London: Geological Society of London), 295–325. doi:10.1144/GOEWP.13

Howard, A. S., Warrington, G., Ambrose, K., and Rees, J. G. (2008). *A formational framework for the Mercia Mudstone Group (Triassic) of England and Wales*, British Geological Survey Research Report, RR/08/004. Nottingham: British Geological Survey.

Insalaco, E., Virgone, A., Courme, B., Gaillot, J., Kamali, M., Moallemi, A., et al. (2006). Upper Dalan Member and Kangan Formation between the Zagros Mountains and offshore Fars, Iran: Depositional system, biostratigraphy and stratigraphic architecture. *GeoArabia* 11, 75–176. doi:10.2113/geoarabia110275

Issautier, B., Viseur, S., Audigane, P., and le Nindre, Y-M. (2014). Impacts of fluvial reservoir heterogeneity on connectivity: Implications in estimating geological storage capacity for CO₂. *Int. J. Greenh. Gas Control* 20, 333–349. doi:10.1016/j.ijggc.2013.11.009

Jenkyns, H. C., Jones, C. E., Gröcke, D. R., Hesselbo, S. P., and Parkinson, D. N. (2002). Chemostratigraphy of the Jurassic system: Applications, limitations and implications for palaeoceanography. *J. Geol. Soc. Lond.* 159, 351–378. doi:10.1144/0016-764901-130

Johnson, D. L., Present, T. M., Li, M., Shen, Y., and Adkins, J. F. (2021). Carbonate associated sulfate (CAS) δ³⁴S heterogeneity across the End-Permian Mass Extinction in South China. *Earth Planet. Sci. Lett.* 574, 117172. doi:10.1016/j.epsl.2021.117172

Jorgensen, B. B., Findlay, A. J., and Pellerin, A. (2019). The biogeochemical sulfur cycle of marine sediments. *Front. Microbiol.* 10, 849. doi:10.3389/fmicb.2019.00849

Korte, C., and Kozur, H. W. (2010). Carbon-isotope stratigraphy across the Permian – Triassic boundary: A review. *J. Asian Earth Sci.* 39, 215–235. doi:10.1016/j.jseaes.2010.01.005

Kovalevych, V., Peryt, T. M., Beer, W., Geluk, M., and Halas, S. (2002). Geochemistry of Early Triassic seawater as indicated by study of the Röt Halite in The Netherlands, Germany, and Poland. *Chem. Geol.* 182, 549–563. doi:10.1016/S0009-2541(01)00343-6

Kubo, Y., Kido, Y., Fuwa, Y., and Hoshino, H. (2016). Experiments on method for washing drill cuttings: Evaluation of soaking, stirring and milling effects. *JAMSTEC Rep. Res. Dev.* 22, 39–48. doi:10.5918/jamstecr.22.39

Kutzbach, J. E., and Gallimore, R. G. (1989). Pangaean climates: Megamonsoons of the megacontinent. *J. Geophys. Res.* 94, 3341–3357. doi:10.1029/JD094iD03p03341

Lott, G. K., and Warrington, G. (1988). A review of the latest Triassic succession in the U.K. sector of the Southern North Sea Basin. *Proc. Yorks. Geol. Soc.* 47, 139–147. doi:10.1144/pygs.47.2.139

Lu, F. H., Meyers, W. J., and Schoonen, M. A. (2001). S and O (SO₄) isotopes, simultaneous modeling, and environmental significance of the Nijar Messinian gypsum, Spain. *Geochim. Cosmochim. Acta* 65, 3081–3092. doi:10.1016/S0016-7037(01)00553-1

Luo, G., Kump, L. R., Wang, Y., Tong, J., Arthur, M. A., Yang, H., et al. (2010). Isotopic evidence for an anomalously low oceanic sulfate concentration following end-Permian mass extinction. *Earth Planet. Sci. Lett.* 300, 101–111. doi:10.1016/j.epsl.2010.09.041

Lyu, Z., Zhang, L., Algeo, T. J., Zhao, L., Chen, Z-Q., Li, C., et al. (2019). Global ocean circulation changes during the Smithian-Spathian transition inferred from carbon-sulfur cycle records. *Earth Sci. Rev.* 195, 114–132. doi:10.1016/j.earscirev.2019.01.010

Markovic, S., Paytan, A., and Wortmann, U. G. (2015). Pleistocene sediment offloading and the global sulfur cycle. *Biogeosciences* 12, 3043–3060. doi:10.5194/bg-12-3043-2015

Márquez-Aliaga, A., Valenzuela-Ríos, J. I., Calvet, F., and Budurov, K. (2000). Middle Triassic conodonts from northeastern Spain: Biostratigraphic implications. *Terra nova.* 12, 77–83. doi:10.1111/j.1365-3121.2000.00273.x

McKie, T. (2017). "Paleogeographic evolution of latest Permian and Triassic salt basins in Northwest Europe," in *Permo-Triassic salt provinces of Europe, North Africa and the Atlantic margins, tectonics and hydrocarbon potential*. Editors J. I. Soto, J. F. Flinch, and G. Tari (Amsterdam, Netherlands: Elsevier), 159–173. doi:10.1016/B978-0-12-809417-4.00008-2

McKie, T., and Williams, B. (2009). Triassic palaeogeography and fluvial dispersal across the northwest European basins. *Geol. J.* 44, 711–741. doi:10.1002/gj.1201

Meshoulam, A., Ellis, G. S., Ahmad, W. S., Deev, A., Sessions, A. L., Tang, Y., et al. (2016). Study of thermochemical sulfate reduction mechanism using compound specific sulfur isotope analysis. *Geochim. Cosmochim. Acta* 188, 73–92. doi:10.1016/j.gca.2016.05.026

Metzger, J. G., Fike, D. A., and Smith, L. B. (2014). Applying carbon isotope stratigraphy using well cuttings for high-resolution chemostratigraphic correlation of the subsurface. *Am. Assoc. Pet. Geol. Bull.* 98, 1551–1576. doi:10.1306/04011412231

Murray, S. T., Higgins, J. A., Holmden, C., Lu, C., and Swart, P. K. (2021). Geochemical fingerprints of dolomitization in Bahamian carbonates: Evidence from sulphur, calcium, magnesium and clumped isotopes. *Sedimentology* 68, 1–29. doi:10.1111/sed.12775

Narkievicz, K. (1999). Conodont biostratigraphy of the Muschelkalk (Middle Triassic) in the central part of the Polish Lowlands. *Geol. Q.* 43, 313–328.

Newell, A. J. (2018). Rifts, rivers and climate recovery: A new model for the Triassic of England. *Proc. Geol. Assoc.* 129, 352–371. doi:10.1016/j.pgeola.2017.04.001

Newell, A. J., and Shariatipour, S. M. (2016). "Linking outcrop analogue with flow simulation to reduce uncertainty in sub-surface carbon capture and storage: An example from the Sherwood Sandstone Group of the Wessex Basin, UK," in *The value of outcrop studies in reducing subsurface uncertainty and risk in hydrocarbon exploration and production*. Editors M. Bowman, H. R. Smyth, T. R. Good, S. R. Passey, J. P. P. Hirst, and C. J. Jordan (London: The Geological Society of London), 231–246. doi:10.1144/SP436.2

Newton, R. J., Pevitt, E. L., Wignall, P. B., and Bottrell, S. H. (2004). Large shifts in the isotopic composition of seawater sulphate across the Permo-Triassic boundary in northern Italy. *Earth Planet. Sci. Lett.* 218, 331–345. doi:10.1016/S0012-821X(03)00676-9

Nielsen, H. (1978). "Sulfur isotopes in nature," in *Handbook of geochemistry*. Editor K. K. Wedepohl (Berlin: Springer), 16.

Noy, D. J., Holloway, S., Chadwick, R. A., Williams, J. D. O., Hannis, S. A., and Lahann, R. W. (2012). Modelling large-scale carbon dioxide injection into the Bunter Sandstone in the UK Southern North Sea. *Int. J. Greenh. Gas. Control* 9, 220–233. doi:10.1016/j.ijggc.2012.03.011

Ortí, F., Pérez-López, A., Pérez-Valera, F., and Benedicto, C. (2022). Isotope composition (δ^{34}S, δ^{18}O) of the Middle Triassic-Early Jurassic sulfates in eastern Iberia. *Sediment. Geol.* 431, 106104. doi:10.1016/j.sedgeo.2022.106104

Parrish, J. T. (1993). Climate of the supercontinent Pangea. *J. Geol.* 101, 215–233. doi:10.1086/648217

Paytan, A., Gray, E. T., Ma, Z., Erhardt, A., and Faul, K. (2012). Application of sulphur isotopes for stratigraphic correlation. *Isot. Environ. Health Stud.* 48, 195–206. doi:10.1080/10256016.2011.625423

Paytan, A., Kastner, M., Campbell, D., and Thiemens, M. H. (2004). Seawater sulfur isotope fluctuations in the Cretaceous. *Science* 304, 1663–1665. doi:10.1126/science.1095258

Paytan, A., Kastner, M., Campbell, D., and Thiemens, M. H. (1998). Sulfur isotopic composition of Cenozoic seawater sulfate. *Science* 282, 1459–1462. doi:10.1126/science.282.5393.1459

Paytan, A., Yao, W., Faul, K. L., and Gray, E. T. (2020). "Sulfur isotope stratigraphy," in *Geologic time scale 2020*. Editors F. M. Gradstein, J. G. Ogg, M. D. Schmitz, and G. M. Ogg (Amsterdam, Netherlands: Elsevier), 1, 259–278. doi:10.1016/B978-0-12-824360-2.00009-7

Peacock, D. C. P. (2004). The post-Variscan development of the British Isles within a regional transfer zone influenced by orogenesis. *J. Struct. Geol.* 26, 2225–2231. doi:10.1016/j.jsg.2004.05.005

Present, T. M., Adkins, J. F., and Fischer, W. W. (2020). Variability in sulfur isotope records of Phanerozoic seawater sulfate. *Geophys. Res. Lett.* 47, e2020GL088766. doi:10.1029/2020GL088766

Present, T. M., Gutierrez, M., Paris, G., Kerans, C., Grotzinger, J. P., and Adkins, J. F. (2019). Diagenetic controls on the isotopic composition of carbonate-associated sulphate in the Permian Capitan Reef Complex, West Texas. *Sedimentology* 66, 2605–2626. doi:10.1111/sed.12615

Present, T. M., Paris, G., Burke, A., Fischer, W. W., and Adkins, J. F. (2015). Large carbonate associated sulfate isotopic variability between brachiopods, micrite, and other sedimentary components in Late Ordovician strata. *Earth Planet. Sci. Lett.* 432, 187–198. doi:10.1016/j.epsl.2015.10.005

Raab, M., and Spiro, B. (1991). Sulfur isotopic variations during seawater evaporation with fractional crystallization. *Chem. Geol.* 86, 323–333. doi:10.1016/0168-9622(91)90014-N

Raup, D. M., and Sepkowski, J. J. (1982). Mass extinctions in the marine fossil record. *Science* 215, 1501–1503. doi:10.1126/science.215.4539.1501

Rennie, V. C. F., and Turchyn, A. V. (2014). The preservation of δ^{34}S$_{SO4}$ and δ^{18}O$_{SO4}$ in carbonate-associated sulfate during marine diagenesis: A 25 Myr test case using marine sediments. *Earth Planet. Sci. Lett.* 395, 13–23. doi:10.1016/j.epsl.2014.03.025

Richardson, J. A., Keating, C., Lepland, A., Hints, O., Bradley, A. S., and Fike, D. A. (2019). Silurian records of carbon and sulfur cycling from Estonia: The importance of depositional environment on isotopic trends. *Earth Planet. Sci. Lett.* 512, 71–82. doi:10.1016/j.epsl.2019.01.055

Richardson, J. A., Lepland, A., Hints, O., Prave, A. R., Gilhooly, W. P., Bradley, A. S., et al. (2021). Effects of early marine diagenesis and site-specific depositional controls on carbonate-associated sulfate: Insights from paired S and O isotopic analyses. *Chem. Geol.* 584, 120525. doi:10.1016/j.chemgeo.2021.120525

Ringrose, P. (2020). *How to store CO$_2$ underground: Insights from early-mover CCS projects*, 129. Switzerland: Springer Briefs in Earth Sciences, Springer Nature. doi:10.1007/978-3-030-33113-9

Salisbury, J., Gröcke, D. R., Cheung, H. D. R. A., Kump, L. R., McKie, T., and Ruffell, A. (2022). An 80-million-year sulphur isotope record of pyrite burial over the Permian-Triassic. *Sci. Rep.* 12, 17370. doi:10.1038/s41598-022-21542-4

Sanei, H., Ardakani, O. H., Akai, T., Akihisa, K., Jiang, C., and Wood, J. M. (2020). Core versus cuttings samples for geochemical and petrophysical analysis of unconventional reservoir rocks. *Sci. Rep.* 10, 7920–8010. doi:10.1038/s41598-020-64936-y

Schobben, M., Stebbins, A., Ghaderi, A., Strauss, H., Korn, D., and Korte, C. (2015). Flourishing ocean drives the end-Permian marine mass extinction. *Proc. Natl. Acad. Sci. U.S.A.* 112, 10298–10303. doi:10.1073/pnas.1503755112

Scholze, F., Schneider, J. W., and Werneburg, R. (2016). Conchostracans in continental deposits of the Zechstein–Buntsandstein transition in central Germany: Taxonomy and biostratigraphic implications for the position of the Permian–Triassic boundary within the Zechstein Group. *Palaeogeogr. Palaeoclimatol. Palaeoecol.* 449, 174–193. doi:10.1016/j.palaeo.2016.02.021

Scholze, F., Wang, X., Kirscher, U., Kraft, J., Schneider, J. W., Götz, A. E., et al. (2017). A multistratigraphic approach to pinpoint the Permian-Triassic boundary in continental deposits: The Zechstein-Lower Buntsandstein transition in Germany. *Glob. Planet. Change* 152, 129–151. doi:10.1016/j.gloplacha.2017.03.004

Schreiber, B. C., and Tabakh, M. E. (2000). Deposition and early alteration of evaporites. *Sedimentology* 47, 215–238. doi:10.1046/j.1365-3091.2000.00002.x

Sepkoski, J. J. (1996). "Patterns of Phanerozoic extinction: A perspective from global databases," in *Global events and event stratigraphy in the Phanerozoic*. Editor O. H. Walliser (Berlin: Springer), 35–51. doi:10.1007/978-3-642-79634-0_4

Smith, D. B. (1989). The late Permian palaeogeography of north-east England. *Proc. Yorks. Geol. Soc.* 47, 285–312. doi:10.1144/pygs.47.4.285

Song, H., Du, Y., Algeo, T. J., Tong, J., Owens, J. D., Song, H., et al. (2019). Cooling-driven oceanic anoxia across the Smithian/Spathian boundary (mid-Early Triassic). *Earth Sci. Rev.* 195, 133–146. doi:10.1016/j.earscirev.2019.01.009

Song, H., Tong, J., Algeo, T. J., Song, H., Qiu, H., Zhu, Y., et al. (2014). Early Triassic seawater sulfate drawdown. *Geochim. Cosmochim. Acta* 128, 95–113. doi:10.1016/j.gca.2013.12.009

Spencer, P. S., and Storrs, G. W. (2002). A re-evaluation of small tetrapods from the Middle Triassic Otter Sandstone Formation of Devon, England. *Palaeontology* 45, 447–467. doi:10.1111/1475-4983.00245

Stuckman, M. Y., Lopano, C. L., Berry, S. M., and Hakala, J. L. (2019). Geochemical solid characterization of drill cuttings, core and drilling mud from Marcellus Shale Energy development. *J. Nat. Gas. Sci. Eng.* 68, 102922. doi:10.1016/j.jngse.2019.102922

Thode, H. G., and Monster, J. (1965). "Sulfur-isotope geochemistry of petroleum, evaporites, and ancient seas," in *Fluids in subsurface environments AAPG Memoir 4*. Editor A. J. E. YoungGalley (Tulsa, OK: American Association of Petroleum Geologists), 367–377.

Trotter, J. A., Williams, I. S., Nicora, A., Mazza, M., and Rigo, M. (2015). Long-term cycles of Triassic climate change: A new δ^{18}O record from conodont apatite. *Earth Planet. Sci. Lett.* 415, 165–174. doi:10.1016/j.epsl.2015.01.038

Tucker, M. E. (1991). Sequence stratigraphy of carbonate-evaporite basins: Models and application to the Upper Permian Zechstein of northeast England and adjoining North Sea. *J. Geol. Soc. Lond.* 148, 1019–1036. doi:10.1144/gsjgs.148.6.1019

Tucker, O. (2018). *Carbon capture and storage*, 46. Bristol: IOP Publishing. doi:10.1088/978-0-7503-1581-4

Van Driessche, A. E. S., Canals, A., Ossorio, M., Reyes, R. C., and García-Ruiz, J. M. (2016). Unraveling the sulfate sources of (giant) gypsum crystals using gypsum isotope fractionation factors. *J. Geol.* 124, 235–245. doi:10.1086/684832

Warren, J. K. (2010). Evaporites through time: Tectonic, climatic and eustatic controls in marine and nonmarine deposits. *Earth Sci. Rev.* 98, 217–268. doi:10.1016/j.earscirev.2009.11.004

Warren, J. K. (2006). *Evaporites: Sediments, resources and hydrocarbons*. Berlin: Springer, 1036. doi:10.1007/3-540-32344-9

Warrington, G. (1974). The stratigraphy and Palaeontology of the 'Keuper' series of the central Midlands of England. *Quart. J. Geol. Soc.* 126, 183–223. doi:10.1144/gsjgs.126.1.0183

Warrington, G. (1997). The Lyme Regis borehole, Dorset – Palynology of the Mercia Mudstone, Penarth and Lias Groups (Upper Triassic-Lower Jurassic). *Proc. Ussher Soc.* 9, 153–157.

Warrington, G., Audley-Charles, M. G., lliott, R. E., Evans, W. B., Ivimey-Cook, H. E., Kent, P. E., et al. (1980). A correlation of Triassic rocks in the British Isles. *Special Rep. Geol. Soc. Lond.* 13.

Warrington, G., and Ivimey-Cook, H. C. (1992). "Triassic," in *Atlas of palaeogeography and lithofacies*. Editors J. C. W. Cope, J. K. Ingham, and P. F. Rawson (London: Geological Society, Memoirs), 13, 97–106. doi:10.1144/GSL.MEM.1992.013.01.11

Warrington, G., and Pollard, J. E. (2021). On the records of the brachiopod '*Lingula*' and associated fossils in Mid-Triassic deposits in England. *Proc. Yorks. Geol. Soc.* 63, 1–9. doi:10.1144/pygs2020-015

Wignall, P. B., and Bond, D. P. G. (2008). The End-Triassic and Early Jurassic mass extinction records in the British Isles. *Proc. Geol. Assoc.* 119, 73–84. doi:10.1016/S0016-7878(08)80259-3

Williams, J. D. O., Jin, M., Bentham, M., Pickup, G. E., Hannis, S. D., and Mackay, E. J. (2013). Modelling carbon dioxide storage within closed structures in the UK Bunter Sandstone Formation. *Int. J. Greenh. Gas. Control* 18, 38–50. doi:10.1016/j.ijggc.2013.06.015

Wilson, A. A. (1993). The Mercia Mudstone Group (Trias) of the Cheshire Basin. *Proc. Yorks. Geol. Soc.* 49, 171–188. doi:10.1144/pygs.49.3.171

Worden, R. H., Smalley, P. C., and Fallick, A. E. (1997). Sulfur cycle in buried evaporites. *Geology* 25, 643–646. doi:10.1130/0091-7613(1997)025<0643:SCIBE>2.3.CO;2

Yao, W. Q., Paytan, A., Griffith, E. M., Martínez-Ruiz, F., Markovic, S., and Wortmann, U. G. (2020). A revised seawater sulfate S-isotope curve for the Eocene. *Chem. Geol.* 532, 119382. doi:10.1016/j.chemgeo.2019.119382

Yao, W. Q., Paytan, A., and Wortmann, U. G. (2018). Large-scale ocean deoxygenation during the Paleocene-Eocene Thermal Maximum. *Science* 361, 804–806. doi:10.1126/science.aar8658

Yao, W. Q., Wortmann, U. G., and Paytan, A. (2019). "Sulfur isotopes – use for stratigraphy during times of rapid perturbations," in *Stratigraphy and timescales*. Editor M. Montenari (Amsterdam: Elsevier Academic Press), 4, 1–33. doi:10.1016/bs.sats.2019.08.004